A Novel Robotic Tree Climbing Mechanism With Anti-Falling Functionality for Tree Pruning

Article *in* Journal of Mechanisms and Robotics · October 2017

DOI: 10.1115/1.4038219

3 authors, including:

Liqiong Tang
Massey University
54 PUBLICATIONS **379** CITATIONS
SEE PROFILE

S.C. Mukhopadhyay
Macquarie University
570 PUBLICATIONS **12,208** CITATIONS
SEE PROFILE

A Novel Robotic Tree Climbing Mechanism With Anti-Falling Functionality for Tree Pruning

Pengfei Gui
School of Engineering and Advanced Technology,
Massey University,
Palmerston North 4410, New Zealand
e-mail: P.F.Gui@massey.ac.nz

Liqiong Tang
School of Engineering and Advanced Technology,
Massey University,
Palmerston North 4410, New Zealand
e-mail: L.Tang@massey.ac.nz

Subhas Mukhopadhyay
Department of Engineering,
Macquarie University,
Sydney 2109, Australia
e-mail: subhas.mukhopadhyay@mq.edu.au

This paper presents a novel mechanism of tree climbing robotic system for tree pruning. The unique features of this system include the passive and active anti-falling mechanisms, which prevent the robot from falling to the ground under either static or dynamic situations, the capability to vertically or spirally climb up a tree trunk, and the flexibility to suit different trunk sizes. The computer-aided design (CAD) models of the robotic mechanism, static and kinematic analysis, climbing simulation, and testing of the physical model are stated in detail. This research work reveals that this novel tree climbing mechanism can be served as a platform for tree pruning robot. [DOI: 10.1115/1.4038219]

Keywords: tree climbing robot, anti-falling mechanism, lightweight, climbing simulation, platform balancing

Introduction

The New Zealand forestry industry makes an important contribution to New Zealand's economy as the third largest export earner [1,2]. To achieve the Wood Council of New Zealand's exports target of $12 billion by 2022 in forest and wood product under the current situation of reduction of harvesting area [1], the unit value and volume of timber must be increased.

Pruning is an essential way to help obtain high quality timber during plantation growing as the pruned lumber can produce a beautiful surface without gnarl and has homogeneous quality with well-formed annual growth ring [3]. High quality pruned stands, well located to the market, could sell for as much as $50,000 per hectare net to the owner, while unpruned stands may net less than $10,000, particularly if logging and cartage cost are high [4]. Currently, almost all the timber pruning work is conducted by lumberjacks. The worker climbs up the tall trunk to cut off branches and gnarl with an axe or chainsaw. This kind of timber pruning method is not only labor intensive and costly but also dangerous and inefficient. Furthermore, the shortage of labor to prune trees will certainly exacerbate this situation [1]. A solution to ease such a situation is through powerful pruning tools and automatic systems. Tree pruning robots therefore become a critical component in sustainable forest management. The major part of a tree pruning robot is the climbing mechanism, which determines how the robot climbs up the tree safely and stably and can identify different climbing pattern for the convenience of pruning. This paper presents a novel design of tree climbing robot which has anti-falling functionality and can climb tree trunks of various diameters vertically or in a spiral pattern. The three-dimensional computer-aided design (CAD) model of the proposed tree pruning robotic mechanism was first created using SOLIDWORKS. Followed was the static and dynamic climbing analysis. Robot climbing simulation was carried out in SIMMECHANICS. Finally, a prototype was built and the experimental results of physical climbing were obtained.

Manuscript received January 15, 2017; final manuscript received September 29, 2017; published online November 29, 2017. Assoc. Editor: Jun Ueda.

Research Status of Tree Pruning Robot

In terms of robot application field, climbing robot is one significant branch. However, the research and development of climbing robots is relatively limited when compared to other robot application areas [3]. The main reason for this status quo is that climbing robots not only need to execute specific tasks in similar fashion to other robotic systems, but are also required to overcome the robot self-weight during the climbing process. For tree climbing robots, the research and study is even less since the climbing environment is more complicated such as the unsmooth surface and irregular shape of the tree trunk. Therefore, to design a mechanism to climb a tree safely, fast, and stably is a challenge. There are only a few tree climbing robot designs available. Their climbing mechanisms can be divided into two types: continuous climb and step-by-step climb.

Wheel mechanism is the most typical style of continuous climb. Kawasaki and coworkers [3,5–7] developed a robot, which can climb up cylindrical objects. It has four wheels in contact with the trunk during climbing. Two of the wheels are located below the robot's center of gravity and adjacent to each other. The other two are installed above the robot's center of gravity. The advantage of this design is that there is no energy consumption when the robot keeps still on the trunk.

Fauroux and Morillon [8] developed a rolling self-locking robot to climb up cylindro-conic poles to perform surveillance and inspection tasks. It utilizes the similar mechanical principle as Kawasaki's design, which can maintain itself at a given altitude on the pole without energy consumption. Using the passive normal force regulation with springs and a force amplifying linkage, it can also climb up a conical pole.

Ahmadabadi and coworkers [9–11] developed a nonholonomic wheel-based pole climbing robot to climb up a lamppost and clean the bulb. This robot employs six single-degree-of-freedom (1DOF) unactuated arms with ordinary 1DOF wheels at their tips to grasp and climb the cylindrical or near cylindrical poles. Three lower wheels are active with the upper ones being utilized to increase the robot stability. It uses the preloaded springs to produce large enough normal components to bring the lower wheels in good contact with the surface of the pole so that the wheels do not slip. This method uses spring mechanism to generate nonautomatically adjustable holding force. In addition, employing 1DOF wheels prevents the robot from climbing the pole in a spiral pattern.

Regarding step-by-step climbing robots, different research projects have resulted in the creation of robots such as RiSE [12,13], Treebot [14], Woody [15], Trepa [16,17], and others [18–20]. The series of RiSE robots are designed for specific tasks such as surveillance, retrieval, and inspection. The latest version of this robot uses four feet with microclaws to climb on textured surfaces. It can climb a telephone pole at a speed of 0.21 m/s with powerful brushless DC motors. However, this robot is not flexible and robust enough to do tree pruning work due to its complex mechanism.

Lam and Xu [14] developed a tree climbing robot inspired by the inchworm. It consists of three components: a front gripper, a continuum body, and a rear gripper. It can do the tree inspection task by climbing from tree trunk to branches with the grippers.

Based on the structure of this robot, it is not suitable for tree pruning work.

The study on existing tree or pole climbing mechanisms shows that for the task of tree pruning, the existing systems are either low speed, nonrobust, or complex mechanisms. Clearly, a tree pruning robot design requires a comprehensive consideration for the climbing mechanism. Also, the total weight of the pruning robot is a major contributor to the climbing system. Furthermore, for any tree climbing robots, the most important feature is that the robot cannot fall to the ground: not only during the climbing process, but also in static situation when the robot remains stationary on the trunk. Among the former mentioned robot designs, some of them can hang themselves on the trunk even if the power is cut off. However, they cannot guarantee the robot not falling during the climbing process caused by the wheel slippage if the holding force between the robot wheel and trunk is unadjustable. Also, due to the unadjustable holding force, the robot flexibility to different diameter of trunks is limited.

Climbing Mechanism Design

Mechanical Construction. The overall mechanical design of the tree climbing robot is shown in Fig. 1. To obtain high climbing speeds, the wheel mechanism is adopted. The design consists of two parts: the platform and the three legs. The pruning tools and the accessories will be added on top of the platform in the future. The platform plays a carrier role, which connects the robot driving system with tree pruning system. It has two parts and is assembled through an open–close joint. Once the robot is set up on the tree trunk, the platform is closed and locked by a specially designed locker.

The robot driving system has three legs evenly distributed under the platform. These legs consist of the driving mechanism, which supports the entire pruning robot. Each leg is composed of four major parts: servomotor, DC motor, linkage, and wheel unit. In addition to these parts, one leg is equipped with a stepper and a screw-nut unit as shown in Fig. 2.

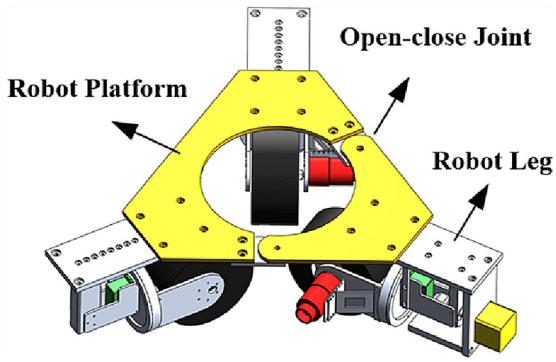

Fig. 1 Mechanical construction of the tree pruning robot design

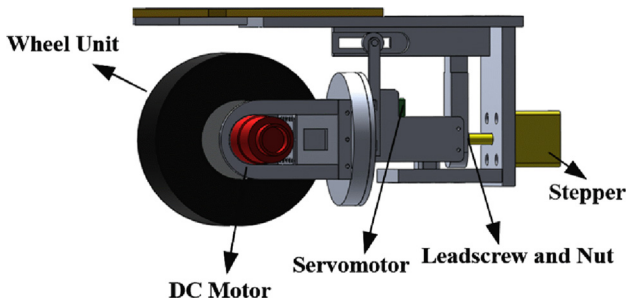

Fig. 2 Climbing robot leg module

This step motor together with the screw-nut unit is the primary mechanism that adjusts the diameter of the circle constructed by the three robot wheels to suit different trunk sizes. In this design, according to the dimension of the screw-nut unit and robot tire sidewall, the trunk diameter that the robot can climb up ranges from 120 to 160 mm. Furthermore, during the climbing process, the stepper can adjust the normal forces between the robot wheels and the tree trunk through the screw-nut mechanism. This holding force adjustment plays a key role in the robot wheel slippage control. The other two legs are fixed legs with a wheel against the tree trunk without installing step motors.

The function of the three servomotors is to change the robot climbing morphology. In addition to vertical climbing, the robot can climb the trunk in a spiral pattern by turning the wheels at given angles. However, during the climbing process, the servomotor may get stuck due to the high normal force between the wheels and the trunk. To solve this problem, a servomotor module is designed, which is illustrated in Fig. 3. This servomotor module consists of three parts: rotary plate, support plate, and lock plate. When the servomotor rotates, the rotary plate connected to the servomotor shaft will force the wheel to rotate. During the servomotor rotating process, the normal force is absorbed by the support plate and the servomotor holding bracket instead of the servomotor shaft. Hence, the servomotor only needs to overcome the friction force between the rotate plate and support plate to swing. The friction force is relatively small compared to the normal force since the contact area between rotary plate and support plate is small and well lubricated.

The three geared motors with encoders provide the power to drive the robot up and down along the tree trunk. Each of the motors has an encoder to control the climbing speed.

Static Analysis in Three-Dimensional Space. The installed one-step motor on one robot leg causes the uneven mass distribution, which leads to the robot center of mass not coinciding with the center of the platform. Thus, under static situations, the platform will be tilted from the horizontal position. This feature allows the climbing robot to have the potential to be able to hang itself on the tree trunk without consuming any power and prevent free falling to the ground when power is cut off.

The step motor can also do fine adjustment to tune the distance between the tree trunk and the tread of the robot wheel, which controls the values of the normal forces applied on the three robot wheels. When the stepper motor moves closer to the tree trunk, the tire contact area with the trunk and the corresponding normal force increase. When the frictional forces obtained by multiplying the normal forces and the friction coefficient overcome the robot gravity force, the robot starts to climb up.

Figures 4 and 5 illustrate the lateral and top view of the forces and moments applied on the robot when it is in static status, and the platform clings to the trunk by gravity without consuming power. The equilibrium status of the forces applied on the robot meet the following conditions:

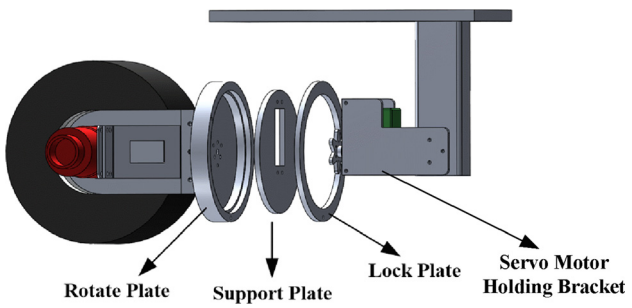

Fig. 3 Servomotor driving mechanism

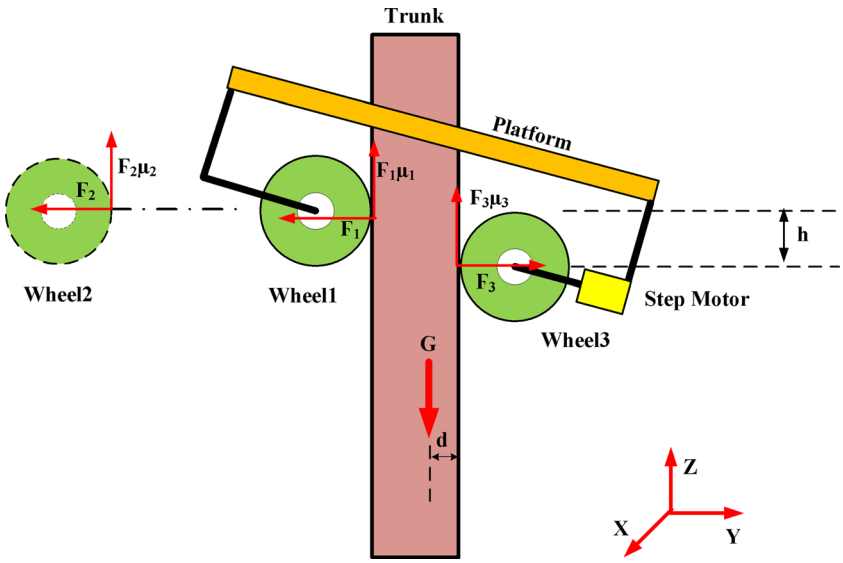

Fig. 4 Lateral view of climbing robot force and moment illustration

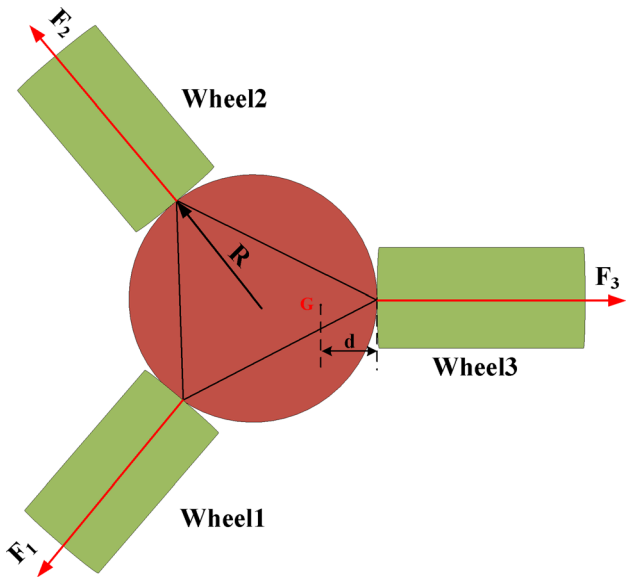

Fig. 5 Top view of climbing robot force and moment illustration

$$\sum F_H = \mathbf{F}_1 \cos 60^\circ + \mathbf{F}_2 \cos 60^\circ + \mathbf{F}_3 = 0 \tag{1}$$

$$\sum F_V = \mathbf{F}_1\mu_1 + \mathbf{F}_2\mu_2 + \mathbf{F}_3\mu_3 = mg \tag{2}$$

where $\mathbf{F}_1$, $\mathbf{F}_2$, and $\mathbf{F}_3$ are the normal forces applied on the three wheels; μ_1, μ_2, and μ_3 are the static friction coefficients; F_H and F_V are the resultant horizontal and vertical forces; and m represents the mass of the robot.

Under equilibrium conditions, assuming wheels 1 and 2 stay at the same level, which is higher than the position of wheel 3, then the equilibrium of the moment at the lower wheel's (wheel 3) contact point gives:

$$\mathbf{F}_1 \cos 60 \deg h + \mathbf{F}_2 \cos 60 \deg h - \mathbf{F}_1\mu_1 \frac{3}{2}R - \mathbf{F}_2\mu_2 \frac{3}{2}R + mgd = 0 \tag{3}$$

where d is the horizontal distance from the surface of the trunk to the robot center of mass, R is the radius of the trunk, and h is the vertical distance between the upper and lower wheels.

Assuming the working condition between the tree trunk and the three wheels is very similar, then $\mu_1 = \mu_2 = \mu_3 = \mu$. According to Eq. (2)

$$(F_1 + F_2 + F_3)\mu = mg \tag{4}$$

From Eq. (1)

$$\frac{1}{2}F_1 + \frac{1}{2}F_2 = F_3 \quad \text{or} \quad F_1 + F_2 = 2F_3 \tag{5}$$

From Eqs. (4) and (5)

$$F_3 = \frac{mg}{3\mu} \tag{6}$$

From the moment equation

$$(F_1 \cos 60^\circ + F_2 \cos 60^\circ)h - (F_1 + F_2)\frac{3}{2}R\mu + mgd = 0 \tag{7}$$

From Eqs. (5)–(7)

$$F_3 h - 3R\mu F_3 + mgd = 0 \tag{8}$$

$$\therefore \mu = \frac{h}{3(R-d)} \tag{9}$$

This means the static friction coefficient can be represented as a function of robot mass center location and the vertical distance between the upper and lower wheels. In this case, to stay on the tree trunk by the robot's own weight without consuming any power, a larger distance between the upper and lower wheels is more desirable.

Dynamic Analysis of Vertical Climbing. For vertical climbing, assuming the stepper shaft is at a proper position, which means no adjustment is needed and the normal forces are big enough to drive the robot up, also assuming the friction coefficient is the same for the three wheels during the climbing process, then the three DC motors that drive the three wheels need to overcome the rolling resistance, robot gravity, acceleration resistance, etc.

Rolling resistance. In this case, the rolling resistance is mainly caused by the hysteresis losses. Assuming the robot wheel is an elastic wheel, which means it can be represented by many micro

spring-damper units. When the wheel tries to rotate on the tree surface, there will be a contact patch generated by the frictional force F_f and resultant normal force F. Once the tire enters the contact patch, these micro spring-damper units are initially compressed and then released. This compress and release process dissipates internal energy in the way of frictional heat and is defined as hysteresis losses.

Figure 6 illustrates the hysteresis losses. Curve A refers to the compress process while curve B is the release process. The area between the curve A and B is the hysteresis losses [21,22].

Robot gravity force. Robot mass is a critical factor in climbing robot design as it directly affects the value of the robot gravity force. Under different circumstances, this gravity force can accelerate or decelerate the robot speed and the mechanical behavior of the mechanism. The total mass of the presented tree climbing robot is approximately 6.42 kg in the CAD design, while the actual total robot mass is 6.8 kg because of the contribution from printed circuit boards and other electrical components.

Acceleration resistance. At the beginning of the tree climbing from a static condition, the three DC motors need to overcome the inertia force caused by the robot mass during the accelerated movement. As shown in Fig. 7, the inertia force is deemed the acceleration resistance F_j

$$F_j = m\frac{dv}{dt} \tag{10}$$

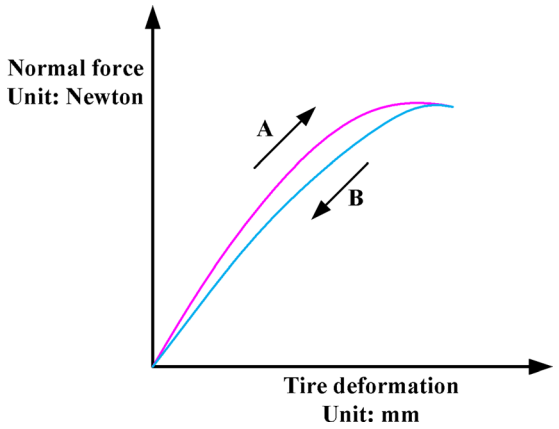

Fig. 6 Climbing robot wheel rolling resistance: hysteresis losses [22]

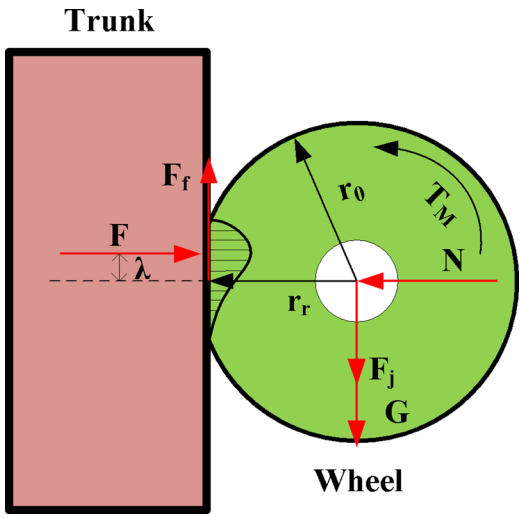

Fig. 7 Force and torque analysis on one robot leg

The inertia torque caused by the acceleration resistance is

$$T_j = I\alpha = F_j r_r \tag{11}$$

where I is the wheel rotational inertia, α is the wheel angular acceleration, and r_r is the wheel rolling radius.

As the robot climbs up, the DC motor's torque should overcome the rolling resistance, robot gravity, and acceleration resistance

$$F_M = F_r + G + F_j \tag{12}$$

$$T_M = T_r + T_G + T_j = F \cdot \lambda + G \cdot r_r + F_j \cdot r_r \tag{13}$$

F_M and T_M are the force and torque required from the DC motor, respectively. T_r is the rolling resistance torque; T_G is the robot gravity torque; F_r is the rolling resistance; G is the robot gravity force; and λ is the vertical offset distance of the resultant normal force F due to the tire deformation.

Active and Passive Anti-Falling Mechanism. This novel tree climbing robot design has a special characteristic: the anti-falling mechanism, both active and passive. The passive anti-falling mechanism uses only friction forces and robot gravity force to maintain a hold on the tree trunk. The primary point of achieving this feature is to let the center of the mass of the robot offset from the center of the tree. The lateral and top views of passive anti-falling mechanism are illustrated in Fig. 8.

During the climbing process, due to the diverse and complicated tree surface, the robot may slip or fall in extreme conditions. Therefore, an active anti-falling mechanism is proposed. As shown in Fig. 4, when the normal forces increase, with the unchanging friction coefficient μ, the total friction force of the robot will be increased correspondingly. This process is executed by the stepper and screw-nut unit. If the stepper motor moves toward the trunk, the normal forces on the wheel–trunk contact areas will be increased. So do the related friction forces. With such an active anti-falling mechanism, it guarantees that the robot can climb up the trunk safely and steadily without slip or falling.

The implementation principle of anti-falling mechanism is that: during the climbing procedure, the active anti-falling mechanism plays the leading role via adjusting the robot holding force while the passive anti-falling mechanism acts as a complement. During the robot spiral climbing, if the robot system loses its power, the active anti-falling mechanism has malfunctioned and the passive anti-falling mechanism takes over to maintain a hold on the tree. This adds an extra layer of support to ensure the robot does not fall during operation. Compared to passive anti-falling mechanism, the main drawback of the active anti-falling mechanism is that it consumes power and requires a dynamic control system.

Simulation and Experiment

The mechanical system of the tree climbing robot was modeled using a CAD system [23]. Each part is assigned with its material property and geometric dimensions in Table 1.

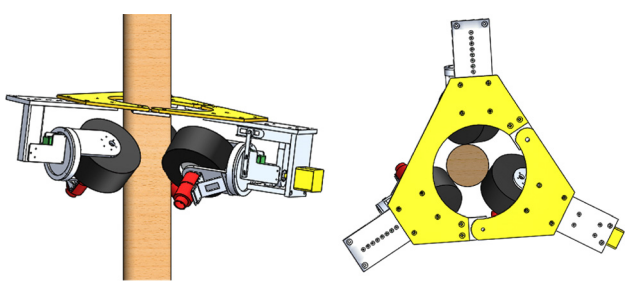

Fig. 8 Passive anti-falling mechanism: lateral view and top view

Table 1 Specification of pruning robot

Parameters	Values
Platform parts mass density	2700 kg/m^3
Wheel mass density	960 kg/m^3
Robot mass	6419.74 g
Volume	3,079,209.1 mm^3
Surface area	1,081,348.83 mm^2

As discussed previously, during vertical climbing process, the wheel tractive force overcomes the rolling resistance, robot gravity, acceleration resistance, motor bearing heat losses, etc. To confirm the previous analysis, the behavior of the climbing robot, and help select the correct motors, a dynamic simulation and analysis of the robot climbing system was conducted using SIMMECHANICS [24] as shown in Fig. 9.

In the dynamic simulation, the inverse kinematic method was used. The wheel rotation angle and rotation speed were set to 4 pi rad and 12 rpm, respectively. To make the simulation more realistic, the slippage and wheel deformation were taken into consideration. Figure 10 showcases the results of required DC motor torque, which is around 1.15 N·m. The corresponding robot vertical climbing speed is shown in Fig. 11. Due to the wheel slippage and deformation, the average robot vertical climbing speed is 62.9 mm/s.

Based on the simulated DC torque and previously dynamic analysis, the DC motor selected in this design is a powerful 12 V

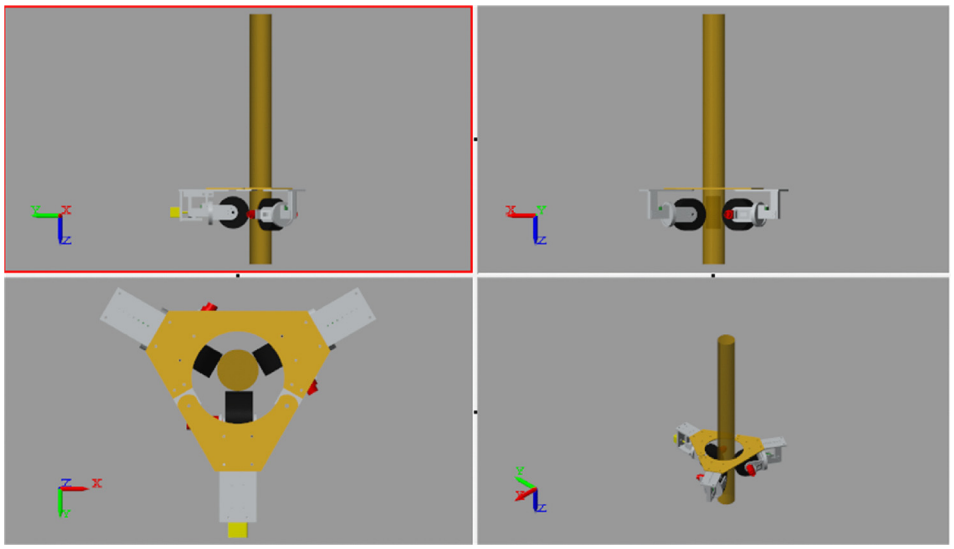

Fig. 9 Four views of pruning robot in SIMMECHANICS

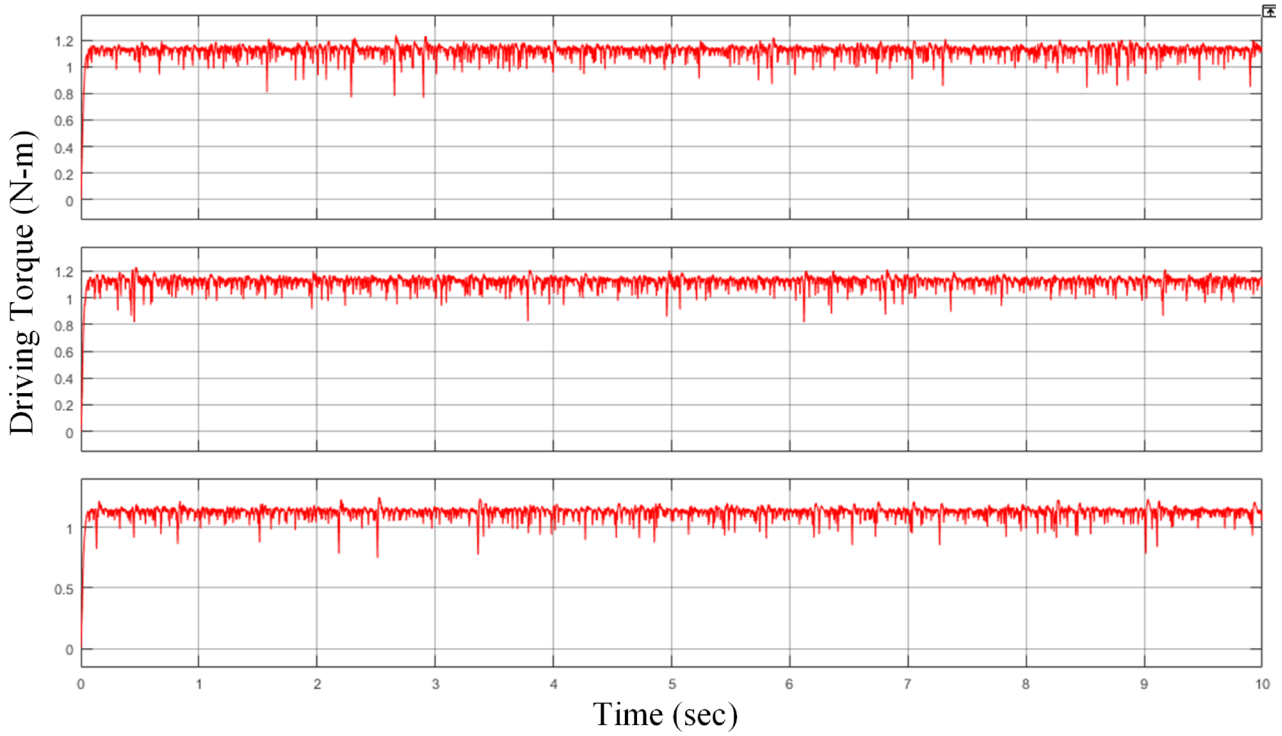

Fig. 10 Direct current motor driving torque

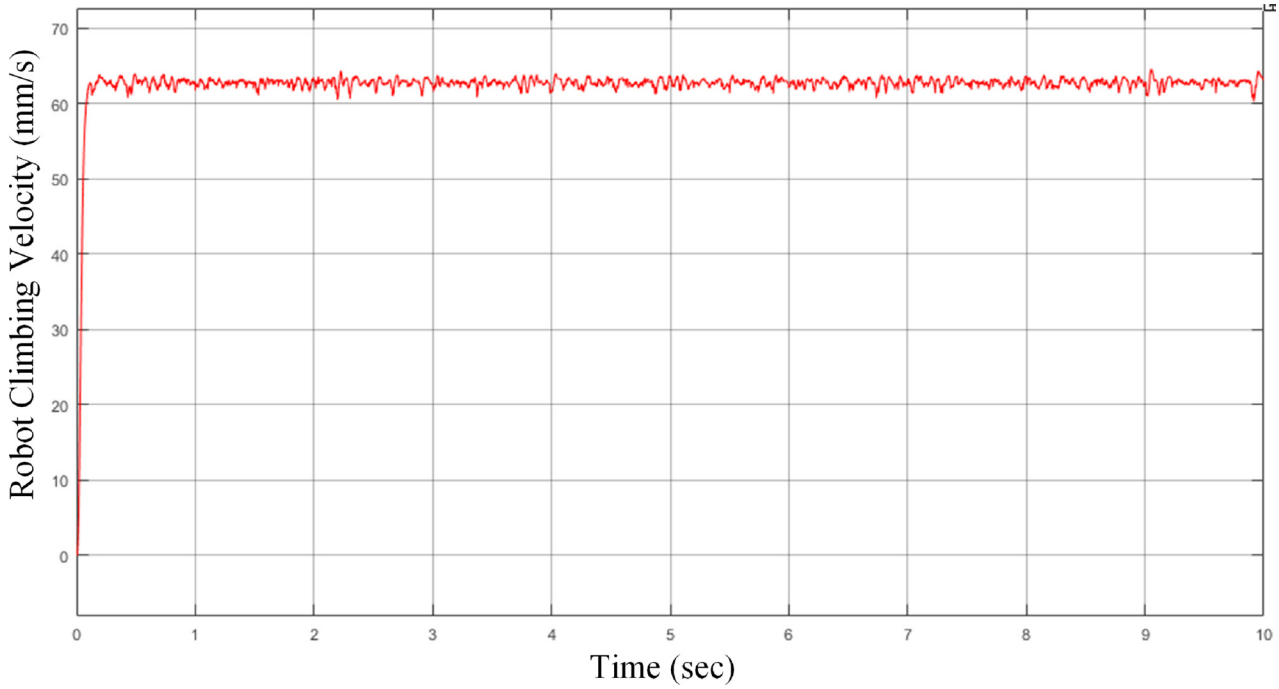

Fig. 11 Robot vertical climbing velocity

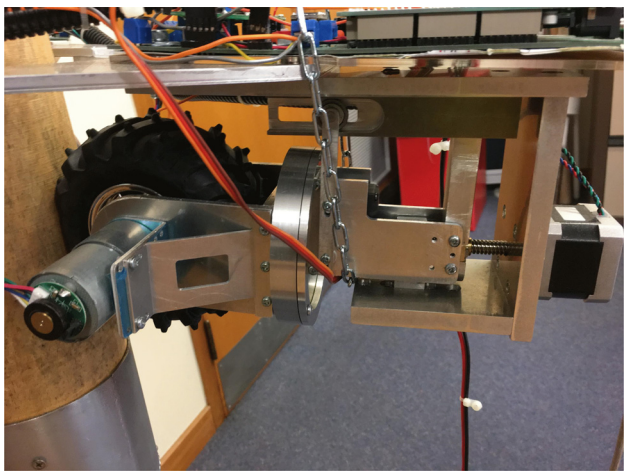

Fig. 12 Tree climbing robot leg

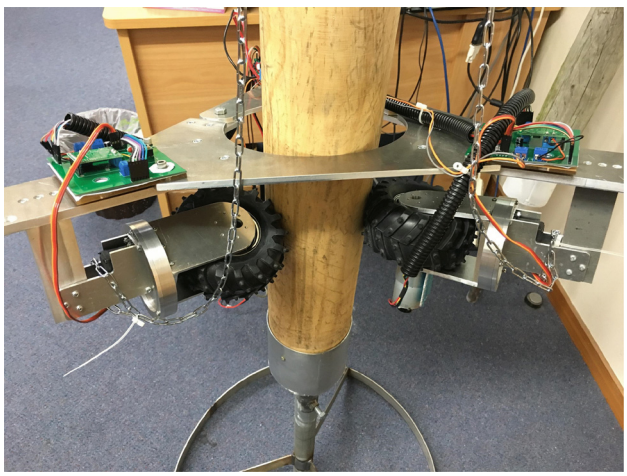

Fig. 13 Tree climbing robot physical test model

brushed DC motor with an integrated quadrature encoder, which can offer maximum 16 kg cm torque.

The friction coefficient between rubber and wood is in the range of 0.75–1 [25]. Based on the robot gravity and previous force analysis, the type of stepper and servomotor was selected. The servomotor used in this design can produce 17 kg cm torque at 6 V. The stepper has 5 kg cm holding torque. The dimension of the robot's rubber wheel is 120 × 60 mm. The first testing climbing robot is then built and shown in Figs. 12 and 13. Figure 12 illustrates the structure of one robot leg while Fig. 13 shows that the robot keeps stationary on the test rod using the passive anti-falling mechanism. The length of the test rod is 1 m and the diameter is 122.5 mm. The total mass of this prototype is 6.8 kg.

In the physical dynamic test, the robot vertical climbing speed is set as 75.36 mm/s (equal to 12 rpm), which is the same as simulated speed. To ensure the robot is climbing safely and steadily, proportion–integration–differentiation control algorithm is adopted to control the three DC motors rotate at the same speed.

Figure 14 is the three DC motors' actual climbing speed on the test rod. Figure 15 shows the relative DC motor current during the climbing process. At time 0, the robot remains motionless on the rod until at time 2, the motor torque is big enough to drive the robot climbing up the pole. The current figure describes and verifies this process. It can be seen from Fig. 14 that the three DC motors' actual climbing speeds are not the same even if the proportion–integration–differentiation control algorithm is employed. This climbing speed difference is mainly caused by wheel slippage since each wheel's friction force varies during the climbing procedure. Therefore, to solve this issue, the robot wheel slippage control algorithm (achieved via stepper and screw-nut unit) needs to design and implement in the future.

Figure 16 displays the testing robot climbing process. In this experiment, the entire robot climbing distance is around 420 mm in 10 s, which means the average climbing speed is about 42 mm/s. This speed is smaller than the simulated climbing speed (around 62.9 mm/s) and setting speed (75.36 mm/s) due to robot wheel slippage and wheel deformation. The maximum load that the robot can take is approximately 2.1 kg at the setting speed of 12 rpm for the DC motors.

The final test result showed that the proposed tree climbing robotic system is able to prevent the robot free fall to the ground

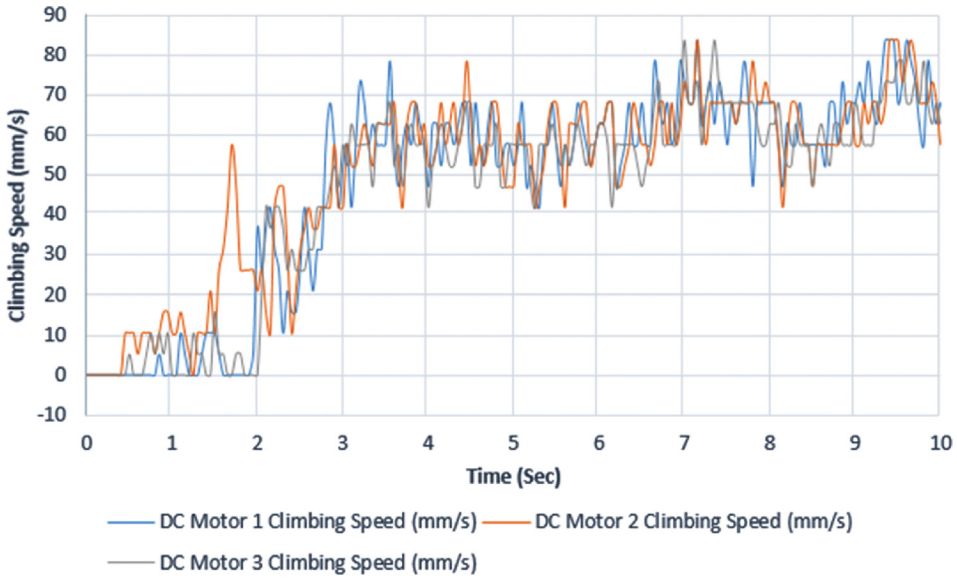

Fig. 14 The three DC motor climbing speed

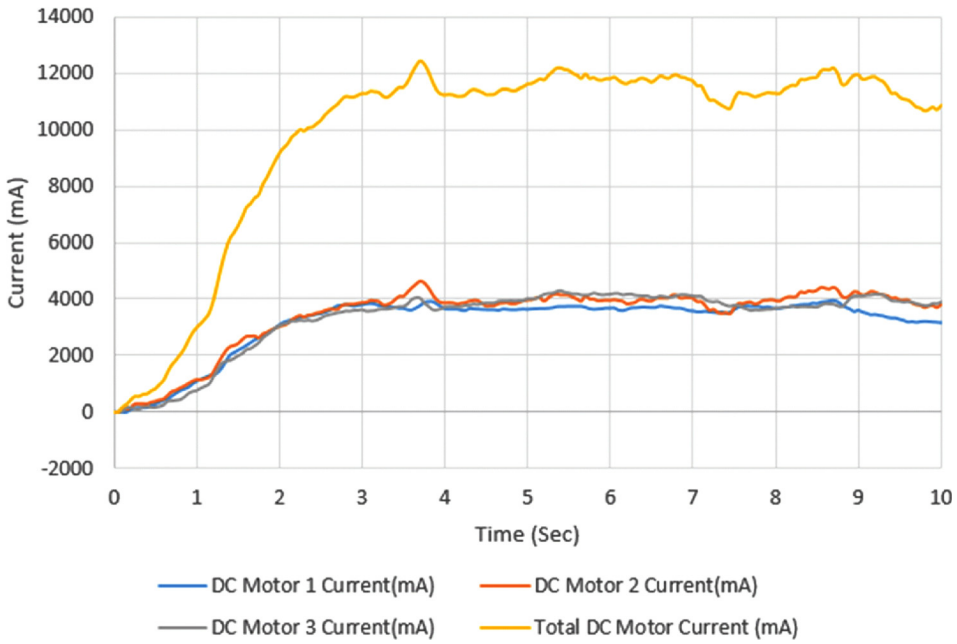

Fig. 15 Direct current motor current

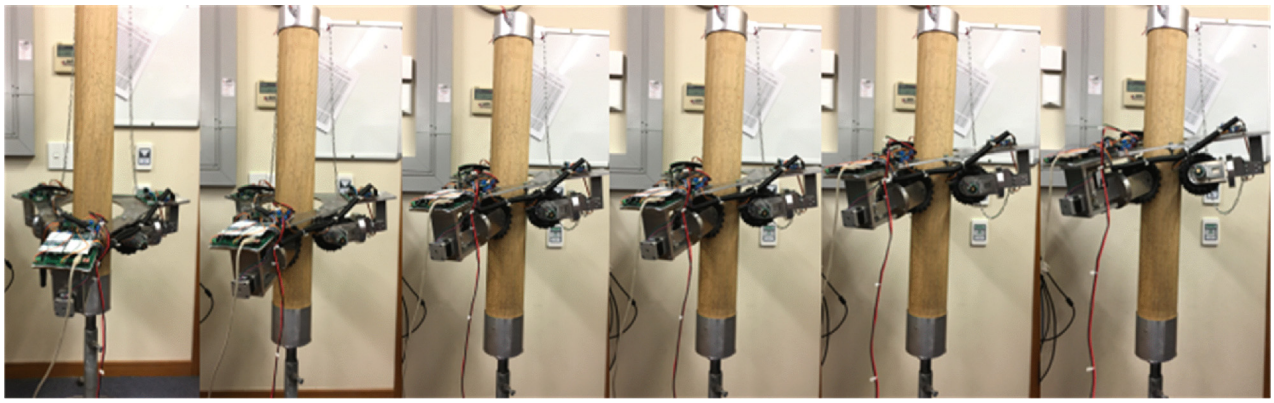

Fig. 16 Tree climbing robot climbing process

under both static and dynamic situations, suit a certain range of trunk diameters, and be served as a base for a tree pruning robot.

Conclusion

A novel tree climbing robot mechanical design and motion simulation has been presented. The main feature of this tree climbing robot is that it implements two sets of anti-falling strategies: passive and active anti-falling mechanisms. The outcome of the robot mechanical analysis and the SIMMECHANICS simulation determines the types of driving mechanism. Then a tree climbing testing model is manufactured and the passive and active anti-falling mechanisms are verified on the test rod. The total weight of this physical model is approximately 6.8 kg and the average vertical climbing speed is 42 mm/s. This climbing velocity meets the design requirement and has potential to be improved if the wheel slippage control algorithm is adopted. Finally, this novel robotic climbing mechanism can be employed as a base for a tree pruning robot.

This research still remains work for further research. For example, during the passive anti-falling test, when the robot remains stationary on the testing rod without power consumption, sometimes the robot wheel will roll back if the servomotor turns the wheel not at a proper angle (DC motor back drive). To completely eliminate this problem, a worm-gear DC motor could be considered. In the dynamic test, when the robot climbs up, the robot platform is tilted and turned around the rod as shown in Fig. 16. This is caused by the robot dynamic tilt and initial setting tilt. In response, an IMU module and wheel slippage control can be integrated to provide a solution to this issue. Furthermore, there are many ways to improve the robot climbing performance such as a further reduction in the weight of the robot by using different materials or reconstructing the robot platform frame, adding intelligent sensing and remote-control modules.

Funding Data

- Massey University (PR40148-1208-GUIPE).

Nomenclature

CAD = computer-aided design
d = the perpendicular distance from the surface of the trunk to the center of mass of the robot
DOF = degree-of-freedom
F = resultant normal force
F_f = static friction force
F_H = the resultant horizontal force
F_j = robot wheel acceleration resistance
F_M = force from DC motor
F_r = robot wheel rolling resistance
F_V = the resultant vertical force
F_1, F_2, F_3 = normal forces applied on the robot wheels
G = robot gravity
h = vertical distance between upper and lower wheels
I = robot wheel rotational inertia
m = mass of the robot
N = applied horizontal force
R = radius of the trunk
r_r = robot wheel rolling radius
r_s = static radius of the robot wheel under loaded condition
r_0 = robot wheel free radius
T_G = robot gravity torque
T_j = robot wheel inertia torque
T_M = torque from DC motor
T_r = rolling resistance torque
α = robot wheel angular acceleration
λ = vertical offset distance of the resultant normal force F due to the tire deformation
μ, μ_1, μ_2, μ_3 = static friction coefficients

References

[1] Goodhew, H. J., 2015, "New Zealand Plantation Forest Industry: Facts and Figures 2014," Forest Owners Association & Ministry for Primary Industries, Wellington, New Zealand, accessed Oct. 23, 2017, https://www.nzfoa.org.nz/images/stories/pdfs/factsandfigures_2014_web.pdf
[2] Goodhew, H. J., 2014, "New Zealand Plantation Forest Industry: Facts and Figures 2012/2013," Forest Owners Association & Ministry for Primary Industries, Wellington, New Zealand, accessed Oct. 23, 2017, https://www.nzfoa.org.nz/images/stories/pdfs/foa_facts_figures_2013.pdf
[3] Kawasaki, H., Murakami, S., Kachi, H., and Ueki, S., 2008, "Novel Climbing Method of Pruning Robot," SICE Annual Conference, Tokyo, Japan, Aug. 20–22, pp. 160–163.
[4] Guy, H. N., 2013, "New Zealand Plantation Forest Industry: Facts and Figures 2011/2012," Forest Owners Association & Ministry for Primary Industries, Wellington, New Zealand, accessed Oct. 23, 2017, https://www.nzfoa.org.nz/images/stories/pdfs/nzf8135_factsfigures.pdf
[5] Chonnaparamutt, W., Kawasaki, H., Ueki, S., Murakami, S., and Koganemaru, K., 2009, "Development of a Timberjack-Like Pruning Robot: Climbing Experiment and Fuzzy Velocity Control," ICCAS-SICE International Joint Conference, Fukuoka, Japan, Aug. 18–21, pp. 1195–1199.
[6] Ishigure, Y., Hirai, K., and Kawasaki, H., 2013, "A Pruning Robot With a Power-Saving Chainsaw Drive," IEEE International Conference on Mechatronics and Automation (ICMA), Takamatsu, Japan, Aug. 4–7, pp. 1223–1228.
[7] Chonnaparamutt, W., and Kawwasaki, H., 2009, "Fuzzy Systems for Slippage Control of a Pruning Robot," IEEE International Conference on Fuzzy Systems, Jeju Island, South Korea, Aug. 20–24, pp. 1270–1275.
[8] Fauroux, J., and Morillon, J., 2010, "Design of a Climbing Robot for Cylindro-Conic Poles Based on Rolling Self-Locking," Ind. Rob., **37**(3), pp. 287–292.
[9] Baghani, A., Ahmadabadi, M. N., and Harati, A., 2005, "Kinematics Modeling of a Wheel-Based Pole Climbing Robot (UT-PCR)," IEEE International Conference on Robotics and Automation (ICRA), Barcelona, Spain, Apr. 18–22, pp. 2099–2104.
[10] Mahdavi, S., Noohi, E., and Ahmadabadi, M. N., 2007, "Basic Movements of a Nonholonomic Wheel-Based Pole Climbing Robot," IEEE/ASME International Conference on Advanced Intelligent Mechatronics, Zürich, Switzerland, Sept. 4–7, pp. 1–6.
[11] Ahmadabadi, M. N., Moradi, H., Sadeghi, A., Madani A., and Farahnak, M., 2010, "The Evolution of UT Pole Climbing Robots," First International Conference on Applied Robotics for the Power Industry (CARPI), Montreal, QC, Canada, Oct. 5–7, pp. 1–6.
[12] Haynes, G. C., and Rizzi, A. A., 2006, "Gaits and Gait Transitions for Legged Robots," IEEE International Conference on Robotics and Automation (ICRA), Orlando, FL, May 15–19, pp. 1117–1122.
[13] Haynes, G. C., Khripin, A., Lynch, G., Amory, J., Saunders, A., Rizzi, A. A., and Koditschek, D. E., 2009, "Rapid Pole Climbing With a Quadrupedal Robot," IEEE International Conference on Robotics and Automation (ICRA), Kobe, Japan, May 12–17, pp. 2767–2772.
[14] Lam, T. L., and Xu, Y. S., 2011, "A Flexible Tree Climbing Robot: Treebot–Design and Implementation," IEEE International Conference on Robotics and Automation (ICRA), Shanghai, China, May 9–13, pp. 5849–5854.
[15] Hiroshi, E., and Yuko, S., 2003, "Robot Assisting Forestry Work," Waseda University, Tokyo, Japan, accessed Oct. 23, 2017, http://www.sugano.mech.waseda.ac.jp/project/forest/index.html
[16] Reinoso, O., Aracil, R., and Saltaren, R., 2006, "A Climbing Parallel Robot: A Robot to Climb Along Tubular and Metallic Structures," IEEE Rob. Autom. Mag., **13**(1), pp. 16–22.
[17] Saltaren, R., Aracil, R., Reinoso, O., and Scarano, M. A., 2005, "Climbing Parallel Robot: A Computational and Experimental Study of Its Performance Around Structural Nodes," IEEE Trans. Rob., **21**(6), pp. 1056–1066.
[18] Lau, S. C., Othman, W. A. F. W., and Bakar, E. A., 2013, "Development of Slider-Crank Based Pole Climbing Robot," IEEE International Conference on Control System, Computing and Engineering (ICCSCE), Penang, Malaysia, Nov. 29–Dec. 1, pp. 471–476.
[19] Guan, Y., Zhu, H., Wu, W., Zhou, X., Jiang, L., Cai, C., Zhang, L., and Zhang, H., 2013, "A Modular Biped Wall-Climbing Robot With High Mobility and Manipulating Function," IEEE/ASME Trans. Mechatronics, **18**(6), pp. 1787–1798.
[20] Tavakoli, M., Lopes, P., Sgrigna, L., and Viegas, C., 2015, "Motion Control of an Omnidirectional Climbing Robot Based on Dead Reckoning Method," Mechatronics, **30**, pp. 94–106.
[21] Zhisheng, Y., 2009, *Automobile Theory*, China Machine Press, Beijing, China.
[22] Zéhil, G.-P., and Gavin, H. P., 2013, "Three-Dimensional Boundary Element Formulation of an Incompressible Viscoelastic Layer of Finite Thickness Applied to the Rolling Resistance of a Rigid Sphere," Int. J. Solids Struct., **50**(6), pp. 833–842.
[23] Dassault Systèmes SolidWorks Corporation, 2015, "Introducing SolidWorks," Dassault Systèmes SolidWorks Corporation, Waltham, MA, accessed Oct. 23, 2017, http://www.solid works.com/
[24] MathWorks, 2007, "SimMechanics 2 User's Guide," The MathWorks Inc., Natick, MA, accessed Oct. 23, 2017, https://mecanismos2mm7.files.wordpress.com/2011/09/tutorial-sim-mechanics.pdf
[25] Roberts, A. D., 1992, "A Guide to Estimating the Friction of Rubber," Rubber Chem. Technol., **65**(3), pp. 673–686.